Submicron electrical current density imaging of embedded microstructures

B. D. Schrag[a)] and Gang Xiao
Department of Physics, Brown University, Providence, Rhode Island 02912

(Received 27 September 2002; accepted 25 February 2003)

We have developed a scanning magnetic microscopy technique for noninvasively imaging submicron magnetic fields from embedded microscopic electrical circuits. We are able to extract from the field data a complete profile of current densities using a mathematical algorithm. As an example, we provide current density images of micron-scale passivated conductors undergoing electromigration. © *2003 American Institute of Physics.* [DOI: 10.1063/1.1570499]

Many physical objects emit characteristic magnetic fields near their surfaces. These fields contain microscopic features and can be weak in strength; however, they reveal quantifiable information about the processes occurring within the object. For example, an integrated circuit (IC) generates an external time-varying magnetic field[1] that reveals the spatial variation of current density in the circuit, while the magnetic image of a recording medium discloses its internal magnetic domain structure.[2] Similarly, one can use magnetic imaging to probe the properties of a superconductor by examining the structure of its threaded flux lines.[3] We have developed a scanning magnetic microscopy technique capable of noninvasively imaging submicron-scale magnetic fields emitted by a current-carrying sample. This technique is capable of extracting a complete profile in-plane current densities in a sample. The excellent spatial resolution and sensitivity of our technique allow submicron detection and isolation of buried features within any circuits. In this letter, we will demonstrate the technique by characterizing the current density profiles of microscopic conductors undergoing electromigration.[4,5] It will be shown that our technique reveals dynamics transparent to traditional imaging methods.

There are many scientific magnetic imaging tools[6–10] available, a handful of which have been considered for the imaging of electrical currents.[11,12] However, these techniques often require specialized conditions (i.e., low temperatures, exposed current-carrying layers), give results which can be difficult to interpret, or lack the necessary resolution. Our technique is noninvasive, operates at ambient temperatures, and can image buried layers with high resolution. The key to the performance of the technique is the use of a nanometer-scale magnetoresistance sensor.[13–15] This nanosensor has an active area measuring tens of nanometers in the primary direction, providing outstanding spatial resolution, has a linear response over a wide frequency range, and is thermally stable.

The physical construction of the microscope is relatively straightforward.[16,17] The sensor is operated in a dc Wheatstone bridge configuration with a constant–current supply. The output of the bridge is passed through a differential low-noise preamplifier and into a lock-in amplifier, whose output is sampled by a 16-bit data acquisition board, as the sensor is rastered continuously across the sample. The sample carries an ac current in the kilohertz region, to which the lock-in is referenced. The microscope operates with the sensor in physical contact with the sample surface, and the entire process is automated using LabVIEW software. The signal-to-noise ratio (SNR) of the technique is dependent on the current density being probed, lock-in parameters, the scanning speed, and, most importantly, the thickness of the dielectric layer between the sensor and current-carrying layers. However, we have achieved SNR$\sim$100 using modulation currents of 1 mA or less. For a conductor with a cross-sectional area of 1×1 μm^2, this represents a current density of 100 kA/cm^2.

As a demonstration, we patterned and scanned numerous current-carrying microscopic conductors with varying geometries. The shape of one such circuit, with a thickness of 0.2 μm and a 0.1 μm SiO_2 overlayer, is shown in Fig. 1(a). A scan of this circuit, carrying a 3 mA modulation current at 80 kHz, yielded the magnetic field profile shown in Fig. 1(b). In this and all subsequent images, the data have been scaled

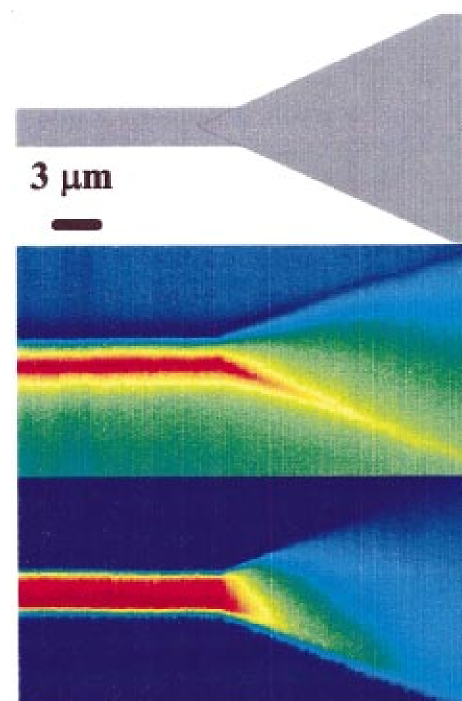

FIG. 1. (Color) (a) Mask template of a 3 μm conductor with a reservoir. (b) Raw magnetic field data of this conductor with a peak-to-peak current of 4 mA. (c) Calculated current density image.

[a)]Electronic mail: schrag@physics.brown.edu

 © 2003 American Institute of Physics
Downloaded 06 May 2003 to 128.148.19.33. Redistribution subject to AIP license or copyright, see http://ojps.aip.org/aplo/aplcr.jsp

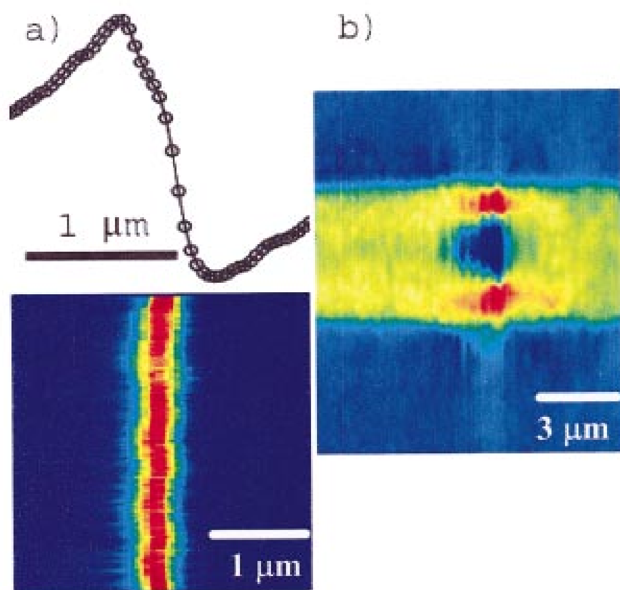

FIG. 2. (Color) (a) Top: magnetic field profile of a 0.4-μm wide conductor. Bottom: current density profile of the same conductor. (b) Current density profile of an unpassivated 5 μm conductor with an electromigration-induced void.

linearly, with dark red representing the largest observed fields (or current densities) and dark blue representing the most negative fields (or current densities). We note that all data presented herein is not massaged or smoothed.

The second part of the technique involves conversion of the out-of-plane field data to an in-plane current distribution, known as the magnetic inverse problem.[18] Roth *et al.* have developed an algorithm for this purpose, and we follow their basic method.[19] They showed that both in-plane components of the current density are determined uniquely with knowledge of any one component of magnetic field. This is accomplished by application of the Biot–Savart law as well as the continuity equation in Fourier space. The effective sensor height, an important parameter for this transform, is calculated by comparison of experimental and analytical results for a current-carrying conductor of known dimensions. Figure 1(c) shows the calculated horizontal component of the current density flowing through the circuit shown in Fig. 1(a).

We patterned conductors with submicron dimensions using electron-beam lithography to test the resolution of the microscope. Figure 2(a) (top) shows the characteristic shape of the magnetic field profile as the sensor scans over a 0.4 μm wide conductor embedded under a 0.1-μm-thick SiO_2 layer, while the bottom figure shows the raw current density profile extracted from the field data. From Fig. 2, we estimate that the spatial resolution is on the order of 40 nm.

This microscopy technique is an ideal tool to study electromigration in miniaturized conductors. We imaged an unpassivated 5 μm wide aluminum conductor after subjecting it to an electromigration stress under a current of 1.5×10^6 A/cm^2 for 4 h. Such a stress caused a 7.5% increase in electrical resistance, and several physical voids were detected in the current density profile of the conductor. A zoomed-in view of one such void is shown in Fig. 2(b). It can be seen that details of the local current density at the submicron level are readily observed. The microscopy can also be used to observe the time evolution of an electromigration process *in situ*. We have obtained a series of images taken on two identical passivated aluminum conductors with lateral dimensions 400×3 μm^2 and a thickness of 0.2 μm. Each sample was deposited via evaporation and covered by a 0.1-μm-thick layer of SiO_2. The conductors, which have triangular metal reservoirs at each end, were subjected to conditions typical of an accelerated electromigration testing environment: a dc current density of 5.8×10^6 A/cm^2 was applied at an ambient temperature of 160 °C. The samples were thermally annealed for several hours at 180 °C before the initial application of current to separate thermal and electromigration effects. For each measurement, the sample was cooled, scanned using the microscope, and the process repeated until the sample failed. The two samples showed strikingly similar void morphologies as electromigration took place. Each showed void formation occurring in two primary areas: in a small ($\sim$15 μm) region of the cathode reservoir, which was the failure site of both samples, and in a longer ($\sim$60–100 μm) section of the conductor near the anode. As a check, the current polarity was reversed for sample B, and the void morphology also reversed. We will present images of cathode voiding taken from sample A and images of the anode region from sample B, although each sample showed qualitatively similar behavior in each region.

A series of images of the current density at the cathode are shown in Fig. 3. These images depict the evolution of

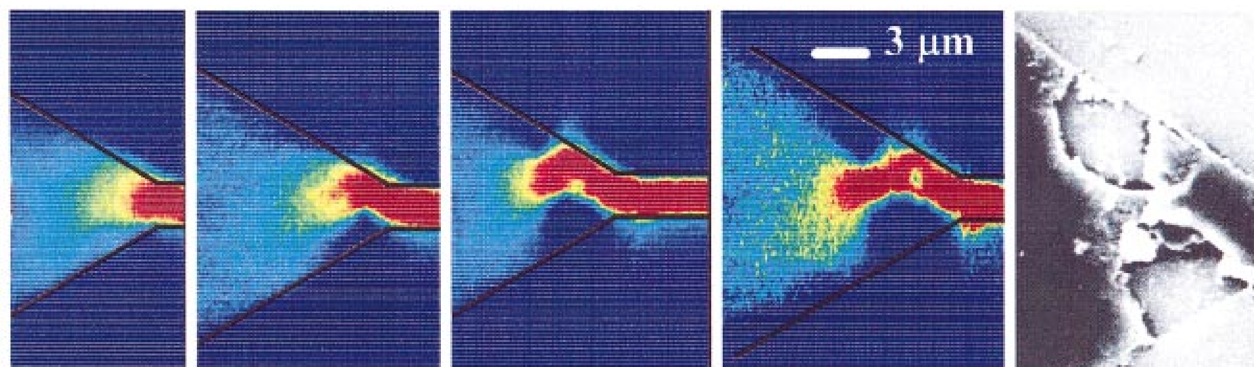

FIG. 3. (Color) (a)–(d) Time evolution of the current density flowing through the cathode of a passivated 3 μm conductor undergoing electromigration. Solid black lines denote the initial edges of the conductor. (e) To the far right is a postmortem SEM micrograph of the stripped sample confirming the failure mechanism.

Downloaded 06 May 2003 to 128.148.19.33. Redistribution subject to AIP license or copyright, see http://ojps.aip.org/aplo/aplcr.jsp

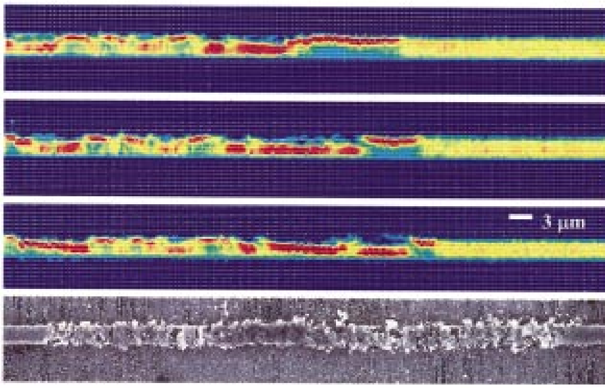

FIG. 4. (Color) A series of images shows void dynamics near the anode of a 3 μm conductor undergoing electromigration. The stressing interval between the first and last images is just over an hour. The bottom image shows a SEM micrograph of the same region in another sample, where the same voiding processes are apparent.

current flow at four stages of accelerated testing, each separated by roughly 3–5 h. The right-most image is a postmortem scanning electron microscopy (SEM) micrograph confirming the failure mechanism. It can be seen that voiding at the cathode nucleates at both edges of the sample at different times, and later a void is seen to nucleate in the center of the cathode. It appears that voiding has already begun at the lower edge of the sample in the first current density image, which was taken 5.7 h after the beginning of the test, indicating that there was little or no incubation time before void formation began. This failure location, which is at a site of large flux divergence, is expected from basic theoretical arguments.

For sample B, the process was slightly different: rather than scanning the sample at regular time intervals, the sample was instead scanned with each 1% increase in resistance. A zoomed-in view of the current density near the anode of sample B is shown in Fig. 4. A large number of voids are observed near the anode, which is located just off the left side of the image. The yellow area of the conductor to the right of the image represents a section of the conductor still undamaged and therefore having a relatively constant current density; the remainder of the conductor, save the cathode, has this same undamaged profile. It can be seen that nearly all the voids appear to nucleate at the top and bottom edges of the conductor. This is expected for electromigration tests at high current densities due to the large thermal gradients occurring at the conductor edges in this regime.[20] In contrast to this, the tests conducted on the unpassivated aluminum conductor revealed a number of voids (one of which is shown in Fig. 2) nucleated in the center of the conductor. In addition, the voids in the unpassivated conductor were more randomly dispersed throughout the conductor, which is also expected for samples with lower current densities.

The sample resistance took 14 hours to increase by 1% initially, but then began to increase much more rapidly, and the next two 1% increments took only an additional 0.3 and 0.9 h, respectively. The current density profiles of the same section of the conductor near the anode after each of these intervals are shown in Fig. 4. The current profiles are similar and show many of the same features, but there are some notable changes. First of all, the voided area is gradually moving towards the cathode, as can be seen from the motion of the right-most voided areas to the right. From these images, we estimate the drift velocity of the damaged area to be 4.5 ± 0.5 μm/h. Second, the void morphology has changed a great deal in the 1.2 h between the first and last image: near the center of the image, it can be seen that the red "hot spots," which indicate where the majority of the current is flowing, have changed as the current alters its path. In the first image, it flows along the top of the conductor for a relatively long distance of ~ 18 μm, while in the second image it flows along the bottom of the film for a longer distance, before "detouring" to flow along the top, and by the third image, it only flows along the top of the conductor for the last 5 μm of voided area. A scanning electron micrograph of the anode region of sample A is shown at the bottom of Fig. 4. The similarity in the morphology between the two samples is readily apparent. It is also interesting to note that the SEM image for the same region of sample B showed no visible damage, perhaps because this sample failed at the cathode before the damage at the anode extended fully through the bulk of the conductor.

In conclusion, we have demonstrated a scanning magnetic microscopy technique for noninvasive detection of electrical currents, based on a nanoscale magnetoresistive sensor. We have explained one promising application of this technique, directly imaging the dynamics of electromigration-induced voiding in fine conductors.

This work is supported by National Science Foundation Grant No. DMR-0071770.

[1] R. Weber, W. Mertin, and E. Kubalek, Microelectron. Reliab. **40**, 1389 (2000).
[2] S. Porthun, L. Abelmann, and C. Lodder, J. Magn. Magn. Mater. **182**, 238 (1998).
[3] C. C. Tsuei, J. R. Kirtley, C. C. Chi, L. S. Yujahnes, A. Gupta, T. Shaw, J. Z. Sun, and M. B. Ketchen, Phys. Rev. Lett. **73**, 593 (1994).
[4] J. R. Black, Proc. IEEE **57**, 1587 (1969).
[5] J. R. Lloyd, J. Phys. D **32**, R109 (1999).
[6] M. R. Scheinfein, J. Unguris, M. H. Kelley, D. T. Pierce, and R. J. Celotta, Rev. Sci. Instrum. **61**, 2501 (1990).
[7] A. M. Chang, H. D. Hallen, L. Harriott, H. F. Hess, H. L. Kao, J. Kwo, R. E. Miller, R. Wolfe, and J. van der Ziel, Appl. Phys. Lett. **61**, 1974 (1992).
[8] D. Rugar, H. J. Mamin, P. Guethner, S. E. Lambert, J. E. Stern, I. McFadyen, and T. Yogi, J. Appl. Phys. **68**, 1169 (1990).
[9] S. D. Bader, J. Magn. Magn. Mater. **100**, 440 (1991).
[10] J. R. Kirtley and J. P. Wikswo, Annu. Rev. Mater. Sci. **29**, 117 (1999).
[11] R. Yongsunthon, A. Stanishevsky, J. McCoy, and E. D. Williams, Appl. Phys. Lett. **78**, 2661 (2001).
[12] L. A. Knauss, A. B. Cawthorne, N. Lettsome, S. Kelly, S. Chatraphorn, E. F. Fleet, F. C. Wellstood, and W. E. Vanderlinde, Microelectron. Reliab. **41**, 1211 (2001).
[13] M. N. Baibich, J. M. Broto, A. Fert, F. N. Vandau, F. Petroff, P. Eitenne, G. Creuzet, A. Friederich, and J. Chazelas, Phys. Rev. Lett. **61**, 2472 (1988).
[14] B. Dieny, J. Magn. Magn. Mater. **136**, 335 (1994).
[15] C. H. Tsang, R. E. Fontana, T. Lin, D. E. Heim, B. A. Gurney, and M. L. Williams, IBM J. Res. Dev. **42**, 103 (1998).
[16] S. Y. Yamamoto and S. Schultz, J. Appl. Phys. **81**, 4696 (1997).
[17] D. K. Petrov, A. Gupta, J. R. Kirtley, L. Krusin-Elbaum, and H. S. Gill, J. Appl. Phys. **83**, 7061 (1998).
[18] See, for example, J. P. Wikswo, Jr., in *SQUID Sensors: Fundamentals, Fabrication, and Applications*, edited by H. Weinstock (Kluwer Academic, The Netherlands, 1996).
[19] B. J. Roth, N. G. Sepulveda, and J. P. Wikswo, J. Appl. Phys. **65**, 361 (1989).
[20] J. R. Lloyd, M. Shatzkes, and D. C. Challaner, Proc. of the IEEE International Reliability Physics Symposium 1988, p. 216.

Downloaded 06 May 2003 to 128.148.19.33. Redistribution subject to AIP license or copyright, see http://ojps.aip.org/aplo/aplcr.jsp